THE JOURNAL OF PHYSICAL CHEMISTRY C
A JOURNAL OF THE AMERICAN CHEMICAL SOCIETY

pubs.acs.org/JPCC

Article

Assessing the Long-Term Reactivity to Achieve Compatible Electrolyte−Electrode Interfaces for Solid-State Rechargeable Lithium Batteries Using First-Principles Calculations

Lieven Bekaert, Ashish Raj, Jean-François Gohy, Annick Hubin, Frank De Proft,* and Mesfin H. Mamme

Cite This: *J. Phys. Chem. C* 2022, 126, 8227−8237

Read Online

ACCESS | Metrics & More | Article Recommendations | Supporting Information

ABSTRACT: Designing compatible electrode−electrolyte interfaces is critical to achieve high and consistent performance and life span in next-generation rechargeable lithium batteries. In the study of nanoscopic interfaces, ab initio molecular dynamics (AIMD) simulations allow for a highly accurate description of interface dynamics and reactions. However, due to the high computational cost, simulations are limited in the size and time domains and therefore merit the need for a new interpretational approach that can deduce the long-term reactivity from such short yet highly accurate simulations. In this study, this is established by means of bond length distribution analysis through which the reactivity of key solid polymer electrolyte (SPE) polymer functional groups in contact with key electrode materials (graphite, silicon, lithium) and the influence of the electric field and temperature was successfully determined. Bond length distributions were found to respond to environmental changes and relate to the long-term reactivity in which the strength of electrode surface interactions and the accessibility of functional groups were found to be critical factors. Furthermore, the balancing of the SPE polymer mobility and functional group−electrode surface attraction, respectively, kinetic and thermodynamic properties, further suggests a selective spatial orientation of functional groups when exposed to an electric field, which could have great implications for low-temperature and high-current-density environments. The obtained knowledge on how reactive key SPE polymer functional groups are and also how their reactivity changes in terms of the electric field orientation effect could provide new insights for designing new stable SPE polymers.

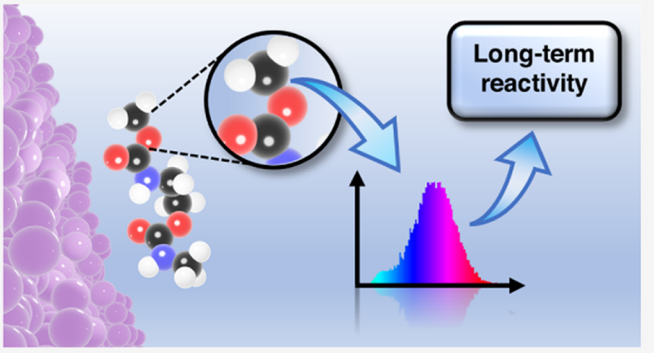

INTRODUCTION

In recent decades, lithium-ion batteries (LIBs) have paved the way for modern electronics and electric vehicles as lightweight, compact, and highly rechargeable energy storage systems.[1] With the rapid boom in the use of LIBs, the limits of this design are being tested, and as a result, several challenges regarding the need for an even greater energy density, safety, performance, and lifespan are speeding up the search for alternative next-generation battery systems.[2] For instance, the use of a lithium metal electrode, which is capable of significantly increasing the energy density, has led to new challenges such as an aggravated passivation layer formation at the electrode−electrolyte interface due to its high reactivity, as well as lithium metal dendrite growth that can lead to short-circuiting and further capacity loss.[3,4]

In an effort to overcome those challenges, solid-state lithium batteries are a promising next-generation alternative in which solid-state electrolytes (SSEs) are used instead of traditional liquid electrolytes, which due to their lower flammability and reactivity have improved safety, reduced electrochemical degradation processes, and further suppressed dendrite formation.[5] However, the high reactivity of several negative electrode materials such as lithium metal[3,4] merits further investigation on the stability of the SSE−electrode interfaces.

With regard to negative electrode materials, the prospect of using lithium metal electrodes is of great interest given the extremely high theoretical energy density of 3860 mAh g^{-1}[6,7] Yet, lithium metal electrodes face the above-mentioned serious issues with a high reactivity and dendrite formation.[4] As a result, lithium-ion insertion materials, including notably graphite, have long been the most popular negative electrode materials for LIB.[8] Even though graphite has a much lower theoretical energy density than lithium metal (372 mAh g^{-1}), it is still preferred for its relative inertness to the electrolyte and the fact that there is very little dendrite growth.[9] On the contrary, silicon has a very high theoretical energy density (~3500 mAh g^{-1}), but the reported volume change upon

Received: February 16, 2022
Revised: April 1, 2022
Published: April 13, 2022

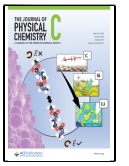

intercalation is very high, up to 420%.[10] As such, various nanostructured[6] and composite[11] materials are being studied, which take advantage of the beneficial properties of the individual materials.

SSE materials have also been undergoing significant improvements and can roughly be divided into two categories.[12] Inorganic solid electrolytes (ISEs)[13] containing more ordered ion conduction pathways have a high ionic conductivity, approaching those of liquid electrolytes,[14] yet face issues with a lower surface wettability and interfacial contact due to their rigidity, which leads to local voids at the electrolyte−electrode interface,[15] as well as a high chemical reactivity, which leads to interfacial decomposition products,[16,17] both of which impede the lithium-ion transport and increase the interfacial resistance, negatively impacting the battery performance. On the other hand, solid polymer electrolytes (SPEs), which consist of a more flexible and loosely connected structure, have a higher surface wettability and interfacial contact but a significantly lower ionic conductivity.[18,19] Hybrid ISE−SPE electrolytes have also been shown to perform well given the balancing of these individual characteristics.[20,21]

Given that SPEs will play a major role in the interface regions, the interactions with the electrode materials will need to be as stable as possible to allow for a long life span and optimal performance, notably at the significantly more reactive negative electrode.[3,4] The characterization of electrode−electrolyte interfaces in batteries at the molecular scale poses significant challenges, in particular through experiments, needing specialized in situ and operando analysis methods and even then still facing space and time limitations.[22] It is here that the strengths of computational atomistic modeling can be demonstrated by understanding this hard-to-access environment.[23] Ab initio molecular dynamics (AIMD)[24] is a widely used computational technique in nanoscale interface modeling with an accurate quantum chemical description allowing for the modeling of dynamics and reactions.[25] However, the higher accuracy increases the computational cost, meaning that simulations can only be run for limited system size (several thousands of cubic Å) and simulation time (several tens of picoseconds), unlike classical molecular dynamics that can accommodate larger systems and timescales although entailing more approximations.[26] As a result, this reduces the chances of observing a reaction within the limited time frame and makes judging the reactivity more challenging.[25] Conventional analysis of simulation results consists among others of comparing bond lengths by means of average values or elongations upon adsorption, whereas in reality, bond lengths oscillate and are expected to be different depending on the interactions at a given time and orientation with respect to the electrode, therefore lacking a holistic insight into the distribution throughout the entire simulation.

With the highlighted developments in both SSEs and negative electrode materials in mind, the insufficiently understood stability of the SSE−negative electrode interface, and the challenges faced with the experimental and computational assessment of this stability, in this study, we propose a new complementary technique in which the distributions of molecule bond length variations are analyzed to predict the long-term reactivity and interactions specific to SPE polymer−negative electrode interface systems. First, the bond length variation technique will be validated by studying the reactivity on lithium for several key functional group types frequently used in SPE polymers (ether, amine, ester, urethane, and alcohol), after which the technique will be applied to assess the influence on the reactivity of several key negative electrode materials (graphite, silicon, and lithium) and the electric field and temperature effect.

METHODS

AIMD simulations were performed using the Vienna Ab initio Simulation Package (VASP) (vasp.5.4.4)[27] using the projector augmented-wave (PAW) method[28] and the Perdew−Burke−Ernzerhof Generalized Gradient Approximation (GGA-PBE) as the exchange-correlation functional.[29] The plane-wave cutoff was set to 550 eV, and a Gaussian smearing with a width of 0.1 eV was used. A 3 × 3 × 1 Monkhorst−Pack k-point mesh was used to sample the Brillouin zone, and the zero damping DFT-D3 method of Grimme was used to account for van der Waals corrections.[30] All simulations were run for 15 000 fs using the Verlet integration algorithm. The temperature was set to 400 K, and the velocities were rescaled every four steps. The electronic self-consistency convergence condition was set to 10^{-5} eV. The mass of hydrogen atoms was changed to that of tritium to increase the timestep to 1 fs.[25] The VESTA software package was used to visualize molecular structures.[31] Bader charge analysis was performed using the Bader package.[32] The three-dimensional (3D) charge density surfaces were generated using VESTA by subtracting the individual charge densities from the combined functional group−electrode charge density ($\Delta\rho = \rho_{\text{molecule+electrode}} - \rho_{\text{molecule}} - \rho_{\text{electrode}}$) while keeping the coordinates same. The iso-surface value was set to 0.002 a_0^{-3} (a_0 is the Bohr radius).

A broad range of common functional group types used in SPE polymers were studied to get a holistic overview: alcohol (R−OH), secondary amine (R_2−NH), ether (R−O−R), ester (R−O−(C═O)−R), and urethane (R−(NH)−(C═O)−O−R). Given the limited system size of AIMD simulations, several small molecules were constructed with several repetitions of the same functional group, to maximize the statistical relevance, as shown in Figure S1 ((pentane-2,3,4-triol, *N*-methyl-*N*′-[(methylamino)methyl] methanediamine, 1,2-diethyoxyethane, methyl 3-(acetyloxy)propanoate, and 2-[(methoxycarbonyl)amino]ethyl methylcarbamate). Structure optimization was performed with the Gaussian 16 program[33] using the density functional theory (DFT) M06/6-31G(d) level of theory with the integral = ultrafine option which has shown to perform well for the studied molecule types.[25,34,35]

Three electrode materials, graphite, silicon, and lithium, were studied in this study given their good prospects of being used as negative electrode materials due to the varied electrochemical properties and theoretical energy densities.[4,6] Graphite (100), silicon (α, 100), and lithium (100) surfaces were constructed consisting of three layers with 36 atoms per layer and of which the bottom layer was fixed. In each simulation, the functional group−electrode distance was 3 Å with a simulation cell size of 25 × 12 × 12 Å^3 including a vacuum space of 15 Å above the molecule to prevent interactions with the electrode base due to the periodic boundary conditions.

In addition, whether a battery is being cycled or not is also an important factor needed to be considered to study the purely "chemical" interactions when not cycling (no external electric field), and the additional "electrochemical" interactions when cycling (with external electric field). All simulations were therefore performed both in the absence and presence of an

https://doi.org/10.1021/acs.jpcc.2c01144
J. Phys. Chem. C 2022, 126, 8227−8237

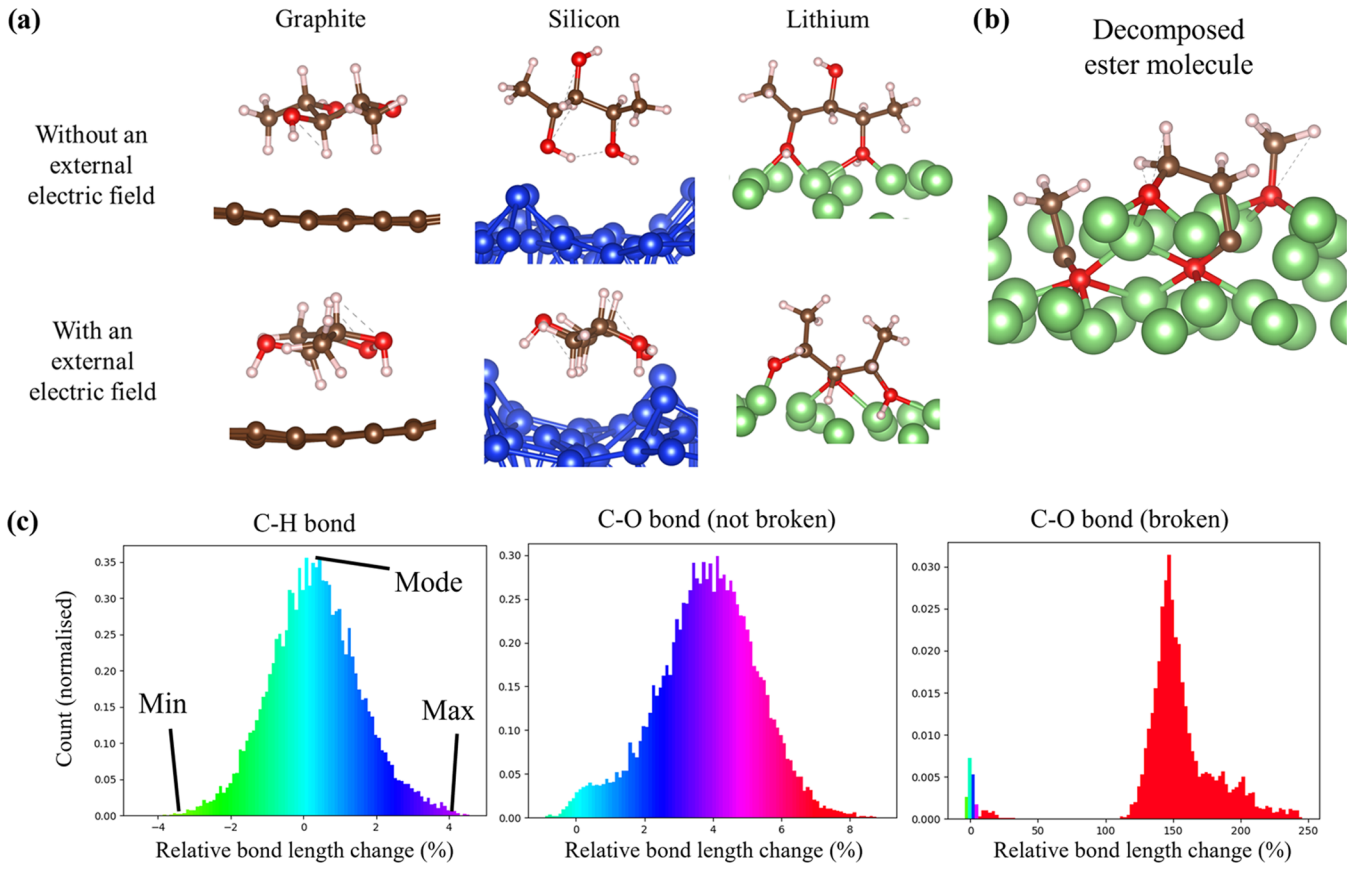

Figure 1. Selected simulation snapshots and bond length distributions. (a) Overview of simulation snapshots for the alcohol molecule. (b) Decomposed ester functional groups on the lithium electrode. (c) RBC distributions for several bond types illustrating the asymmetry and statistics used to compare the distributions (minimum, maximum, and mode).

external electric field of 0.3 V/Å, which is in a realistic range for lithium batteries.[36]

As an experimental validation alongside findings in the literature, a poly(hydroxyurethane)-LiTFSI SPE containing all of the bond types considered in this study (molecular structure shown in Figure S2) was cycled in a symmetrical lithium metal electrode cell with a PTFE ring (CR2032) for 100 h/50 cycles at 5 μA with a cutoff potential of +4/−4 V at 60 °C in a climate chamber using a BioLogic VMP3 multichannel potentiostat. Angle-resolved X-ray photoelectron spectroscopy (ARXPS) was performed using an SSI X-Probe (SSX 100/206) photoelectron spectrometer from Surface Science Instruments with a monochromatized Al Kα X-ray source (200 W, width 800 μm × 800 μm). ARXPS was performed at the angles of 15, 35, and 55° to obtain depth profiles. High-resolution XPS measurements were also conducted for pristine lithium metal and pristine poly(hydroxyurethane)-LiTFSI SPE for reference on the same instrument. All of the binding energies were calculated according to the C-(C,H) component of the C 1s peak fixed at 284.8 eV. Data analysis was carried out using CasaXPS software. For the survey scan, a 1.0 eV step size was used and a 0.1 eV step size was used for high-resolution scans for all elements with 150 energy steps.

It was hypothesized that upon exposure of a molecule to an electrode surface, bonds could either respond by stretching more due to beneficial interactions with the electrode or compress more due to repulsion with the electrode. An increased bond length could lead the bond to break or allow the bonding electrons which are then more exposed to rearrange, ultimately leading to a reaction. This information could then be used to predict the long-term reactivity of bonds and the corresponding functional groups, thus overcoming the time domain limitations of AIMD simulations. Because equilibrium bond lengths vary depending on the type of bond, and to observe changes induced by interactions with the electrode surface, the bond lengths were normalized with respect to the values obtained in the first AIMD timestep in which the molecule is at a sufficient distance from the electrode surface and assumed noninteracting. The corresponding "relative bond length change" (RBC) is then calculated as $((\mathrm{BL}(t)/\mathrm{BL}(0)) - 1) \times 100\%$, where $\mathrm{BL}(t)$ is the bond length at any given time and $\mathrm{BL}(0)$ is that of the first timestep. Positive values indicate more relative stretching of the bond, and negative values indicate more compression of the bond, which are expected to indicate higher and lower reactivities, respectively. This differs from the radial distribution function in that the RBC involves not only the coordination but also indicates the reactivity.

RESULTS AND DISCUSSION

In all simulations, the functional groups approached the electrode surface but differed in the subsequent interactions. On graphite, there was a significant continuous rotation and movement over the surface, whereas on lithium, functional groups remained in place due to stronger local interactions. On silicon, an intermediate behavior was observed. The presence of an electric field resulted in a smaller molecule−electrode distance and changes in the orientation of bonds with respect

https://doi.org/10.1021/acs.jpcc.2c01144
J. Phys. Chem. C 2022, 126, 8227−8237

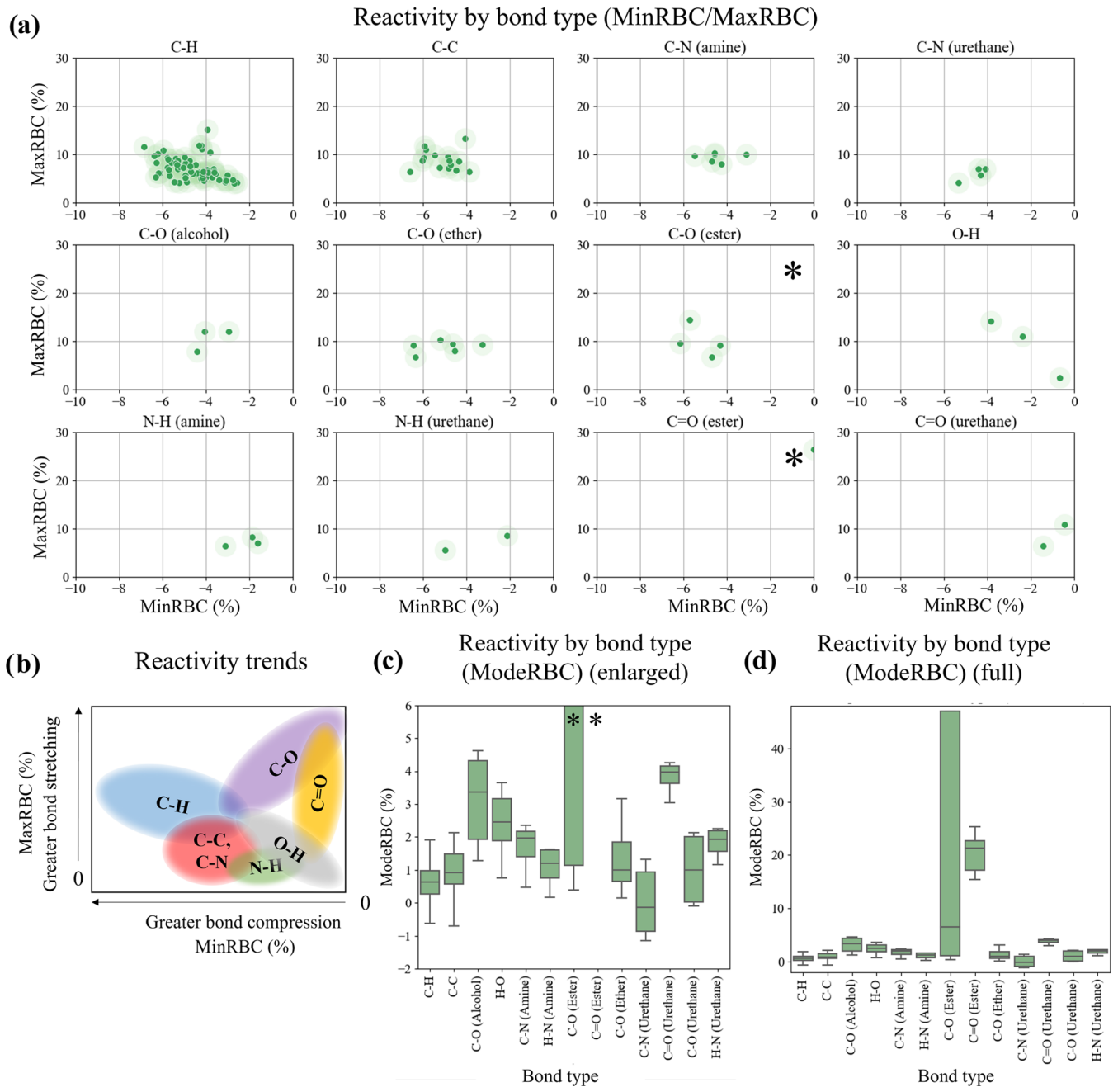

Figure 2. Bond-type reactivity comparison. (a) MinRBC/MaxRBC plots for all bond types on a lithium metal electrode. Asterisks indicate that several points from the lithium electrode simulations lay outside the plot area, up to 250% MaxRBC for the same MinRBC range. (b) Schematic summary of the characteristic bond-type reactivity based on (a). (c) ModeRBC variations between all bond types on a lithium metal electrode. The ModeRBC axis range was limited for improved visibility; the full plot is shown in (d).

to the surface. An example of the interactions with the electrode for the alcohol molecule in the presence and absence of an electric field is shown in Figure 1a. Out of all simulations, regardless of the presence or absence of an electric field, only one type of reaction was observed (Figure 1b) in which the ester molecule decomposed on the lithium electrode, during which the ethereal C−O bond broke to form alkoxide species. As was anticipated, the limited simulation time limits the number of observable reactions. A further investigation is thus needed to estimate the long-term reactivity for all functional groups aside from solely judging from visually observed bond breakages.

To do this, the distributions of the relative bond length change (RBC) of individual bonds were analyzed. RBC values were obtained from processing all combined timesteps in all simulations excluding the first femtosecond to avoid artificial surface placement artifacts using the equation explained in the methodology section. Figure 1c shows several selected examples of distributions for a C−H, single unbroken C−O, and broken C−O bond. The C−H bond, which is known to be a chemically stable bond type in the context of batteries,[37] shows a symmetrical, normally distributed distribution in which the symmetry is caused by the natural bond length oscillation. The absence of any asymmetry indicates that this particular C−H bond did not change in its oscillation

https://doi.org/10.1021/acs.jpcc.2c01144
J. Phys. Chem. C 2022, 126, 8227−8237

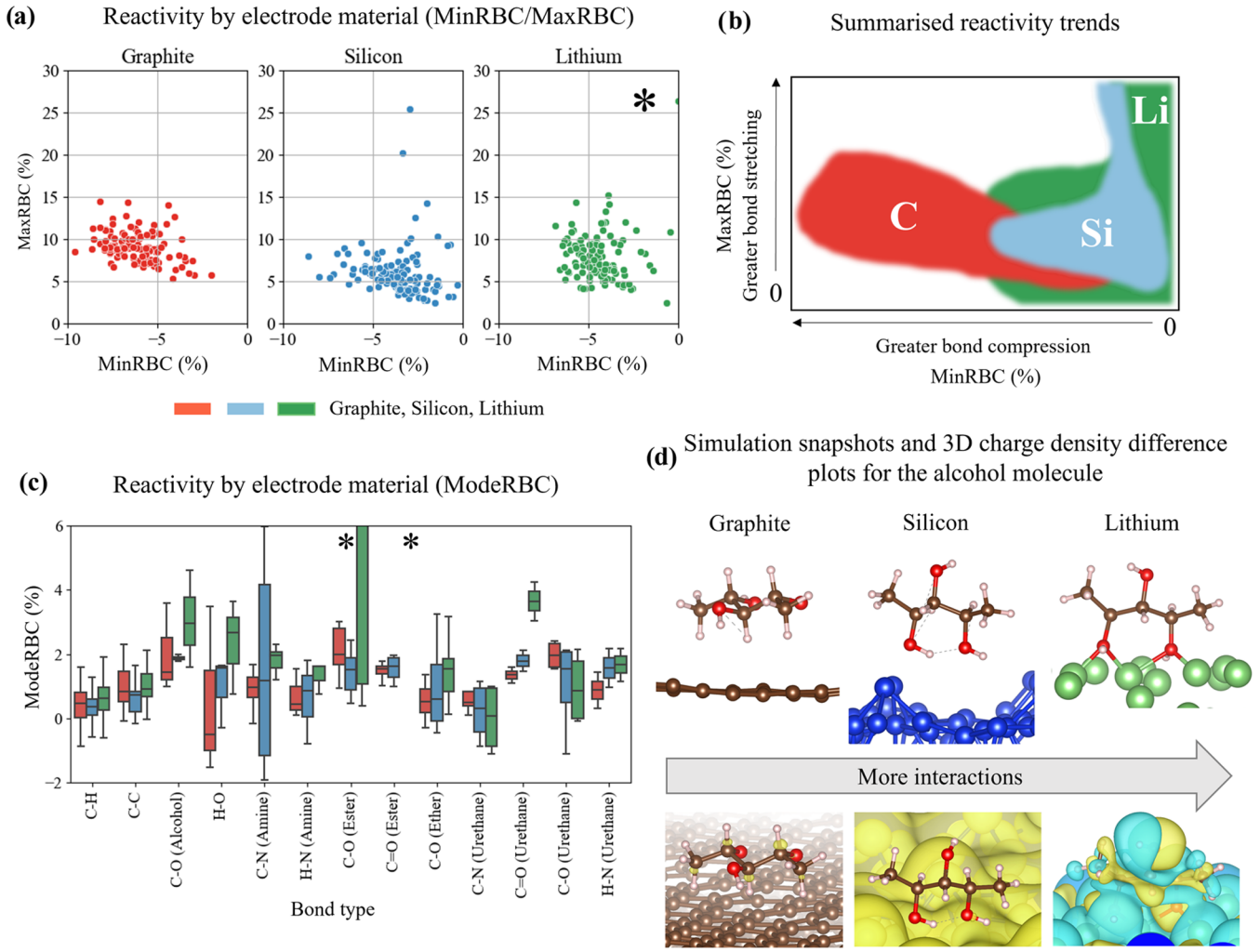

Figure 3. Electrode material reactivity comparison with simulation snapshots. (a) MaxRBC/MinRBC plots for all bond types combined for each electrode material. Red, blue, and green indicate the simulations on graphite, lithium, and silicon, respectively. The asterisk indicates that some points up to 250% MaxRBC and within the same MinRBC are also present outside the plot. (b) Schematic summarizing the characteristic electrode material reactivity based on (a). (c) ModeRBC plots for all bond types on all electrode materials. The asterisks indicate that for lithium, the average values were close to 6% and lie outside the plot (shown in Figure S7). (d) Simulation snapshots (top row) and 3D charge density difference plots (bottom row) for the alcohol molecule on all electrode materials to illustrate the degree of molecule−electrode interactions. Yellow indicates a charge accumulation, and blue indicates a charge decumulation.

throughout the simulation, suggesting no particular interactions. On the other hand, the unbroken C−O bond shows an asymmetry, indicating that at a given time, the bond shifted toward a greater interaction with the electrode surface, which caused its equilibrium bond length to increase to 4%. Finally, the broken C−O bond shows an even greater asymmetry with the largest peak near 150%, indicating that the bond broke and remained in this state for a considerable fraction of the simulation. Due to the presence of asymmetries in the distributions and the fact that the distributions are no longer normally distributed, statistics such as the average and standard deviation cannot be used to describe the RBC distribution.[38] Instead, the following three statistics were used as indicated in the figure: (1) the minimum (MinRBC), which indicates the greatest compression experienced by the bond, (2) the maximum (MaxRBC), which indicates the greatest stretching experienced by the bond, and (3) the mode (ModeRBC), which indicates the most common RBC state of the bond. An increase (and less negative values in the case for the MinRBC) in either of these three statistics is then hypothesized to signify a greater reactivity given the longer bond length which allows for greater exposure of the bonding electrons to the electrode as well as other surrounding species.

Bond Lengths Respond to Environmental Changes. First, the reactivity of the individual functional groups was assessed on a lithium metal electrode using the above-mentioned parameters derived from the RBC distributions. For clarity, first, the nonelectric field results will be discussed. To observe the relative compression and stretching characteristics for each bond type, the MinRBC was plotted versus the MaxRBC in Figure 2a and the ModeRBC was plotted in Figures 2c,d.

Bonds with a shorter bond length and low degree of polarization were found to exhibit a lower reactivity as indicated by a more negative MinRBC and smaller MaxRBC and ModeRBC. This was notably the case for C−H bonds, which have been shown to be stable toward a lithium metal electrode.[37] C−C bonds were found to be in the same region as C−H bonds although with less compression, due to being part of the molecule backbone and shielded from interactions

https://doi.org/10.1021/acs.jpcc.2c01144
J. Phys. Chem. C 2022, 126, 8227−8237

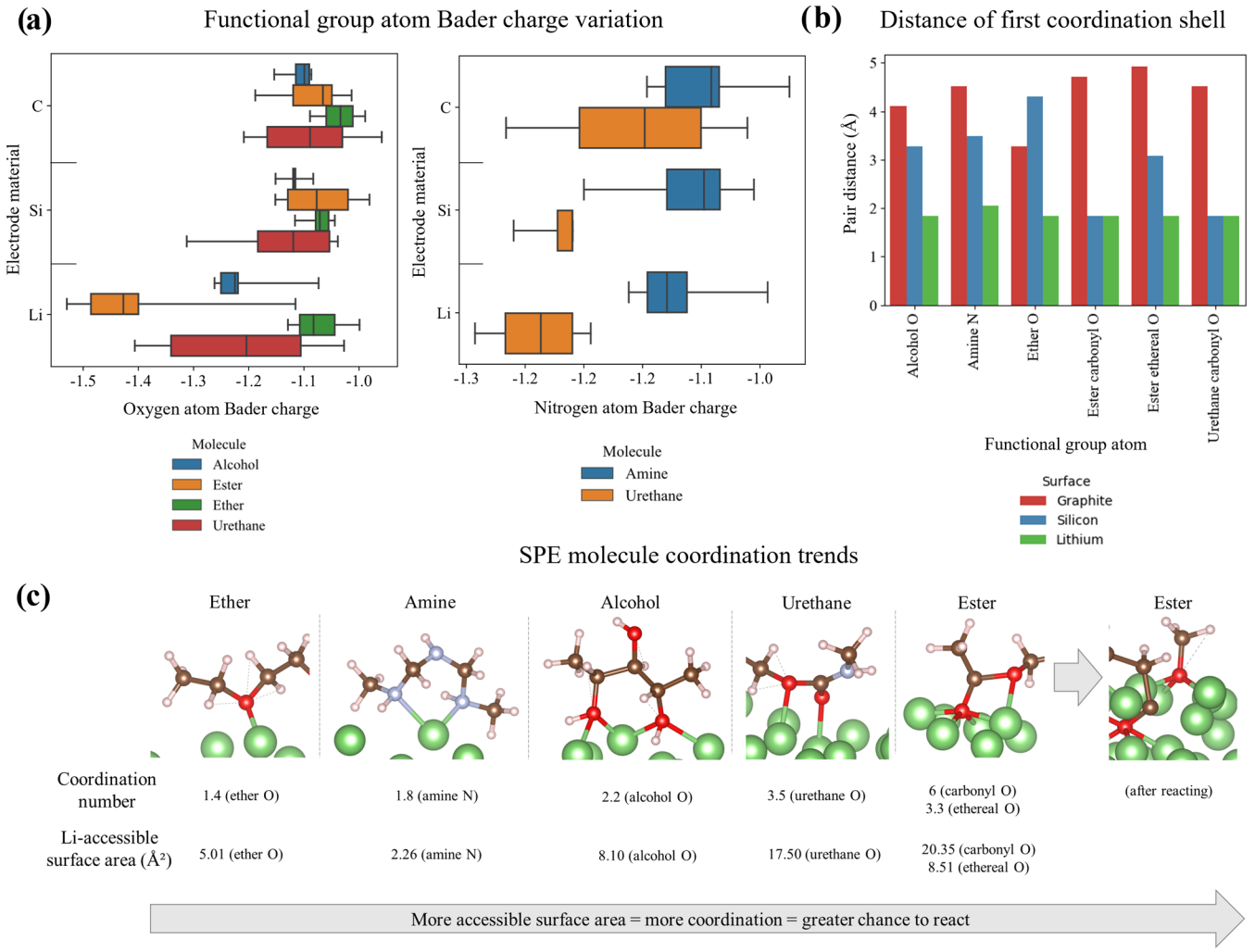

Figure 4. Functional group coordination by electrode atoms. (a) Bader net atomic charges for all oxygen and nitrogen atoms in all functional groups when placed on different electrode materials. (b) Distance to the first coordination shell of all key functional group atoms on all electrode materials. The urethane ethereal oxygen and nitrogen atoms are not included due to their absence in the first coordination shell. (c) Simulation snapshots for all functional groups on lithium prior to any reactions. The coordination number and lithium-accessible surface area (Å^2) are shown below. The decomposed ester group is shown to the right, being the only functional group that reacted within the 15 ps simulation time on lithium.

with the electrode. N−H bonds experienced less compression than C−H and C−C bonds given the greater degree of bond polarization but also due to the N atom which has been found to have a high affinity to lithium atoms.[39] O−H bonds were found to have the combined smallest MinRBC and MaxRBC, which is expected to be due to the O−H bond being more polarized and/or the O−H group sticking out of the backbone in the alcohol molecule (unlike the N−H bond in which the N atom is part of the backbone in the molecules used in this study), which allow for more interactions with the electrode surface. While there were no species present in the simulation to deprotonate the hydroxyl group, bases present in solid−electrolyte interphases can deprotonate the hydroxyl group to form alkoxides and would be expected to further increase the MaxRBC.[25] Single C−O and C−N bonds were found to have an intermediate MinRBC and a greater MaxRBC, notably for C−O bonds given their longer bond length and greater bond polarity, in particular stretching up to 250% for the ester functional group, and thus breaking (Figure 1b). This reaction has been widely reported in the literature for ester and carbonate electrolytes.[4,25,40,41] Carbonyl C═O bonds were found to stretch up to 30% in MaxRBC yet did not break due to the stronger double-bond nature; this was also confirmed by another study,[25] although nucleophilic attacks on the carbonyl C atom by lithium hydroxides or alkoxides present at the interface could potentially decompose the ester groups. Due to the lower accessibility of the functional group atoms in the ether molecule and the delocalization in the urethane molecule, the C−N and C−O ModeRBC values were lower than those of the more accessible functional groups. The resulting approximate trends are summarized in Figure 2b. As such, C−H, C−C, and C═O bonds were found to have the lowest reactivity and single C−O and C−N bonds are expected to have the greatest reactivity.

Because the referenced studies considered SPE polymers each containing only one functional group type, the degradation products of a poly(hydroxyurethane)-LiTFSI SPE collectively containing the same functional groups considered in this study were experimentally assessed using angle-resolved XPS (Figures S3−S6). Decomposition was found to be greater in cycled cells than those stored at OCP, confirmed by comparing with clean Li and SPE spectra. LiTFSI decomposition products were observed, indicated by the presence of LiF, Li3N, and S−O (−SO3) peaks on F 1s, N

https://doi.org/10.1021/acs.jpcc.2c01144
J. Phys. Chem. C 2022, 126, 8227−8237

1s, and S 2p spectra, respectively. The formation of alkoxide, carbonate, and organic C−(H,C) substances arising from SPE degradation was confirmed on cycled and OCP samples as indicated by a significant rightward shift and peak broadening in O 1s spectra as well as the presence of C−(C,H), C−O, O−C−O/C═O, and O−(C═O)− on C 1s spectra. Moreover, on the cycled lithium electrode, the C═O, O−C−O peak was significantly more pronounced than on the lithium electrode stored at OCP, indicating more decomposition of ester and potentially urethane species as a consequence of electrochemical reactions. The predictions that we have made using the newly developed bond length variation distribution analysis are therefore consistent with experimental and computational studies[4,25,37,39,40] and confirm that the approach which we have proposed is capable of predicting the long-term chemical and electrochemical reactivity of electrolyte−electrode interfaces.

Influence of Negative Electrode Materials on the Reactivity. Given the validation of the technique, bond length distribution analysis was subsequently performed to investigate the reactivity on other key electrode materials (graphite and silicon). All bond types were combined per electrode material to clarify the overall relative shifts in reactivity in terms of the MinRBC/MaxRBC (Figure 3a) and ModeRBC (Figure 3c). Comparing the relative locations as summarized in Figure 3b, functional groups exposed to a graphite surface showed a greater bond compression (more negative MinRBC), indicating a lower reactivity and greater repulsion to the electrode. The observed upward trend toward the top-left corner is due to the more extreme bond length oscillations as a result of a greater compression and expansion arising from the repulsion of the flat graphite surface. This may indirectly cause an increase in the reactivity due to the dynamism of the bond. Functional groups exposed to silicon and lithium surfaces both showed a less negative MinRBC and a higher MaxRBC, particularly for lithium, indicating a greater reactivity. Taking into account the lower accessibility of the functional group atoms in the ether molecule and delocalization in the urethane molecule, the trends in ModeRBC also indicate a relative increase in reactivity from graphite toward lithium.

To explain and relate the observed reactivity trends to structural properties, snapshots and 3D charge density difference plots for the alcohol functional groups are shown in Figure 3d (other molecules are shown in Figures S8−S12). Although the molecule is found to align parallel to the graphite electrode, on silicon, several of its hydroxyl groups are facing toward the silicon surface, and on lithium, the hydroxyl groups are even more strongly interacting with the electrode surface. On the 3D charge density difference plots, an increase from graphite toward lithium as indicated through the presence of more charge depleted and enriched areas confirms the increase in interaction. The same trends were observed for all other molecules. Bader net atomic charge analysis (Figure 4a) showed the net atomic charge of oxygen and nitrogen atoms in all molecules becoming more negative when going from the graphite to the silicon and then lithium metal surface, which indicates that relatively more electrons from the electrode surface have a greater affinity for the oxygen and nitrogen atoms. It is hypothesized that the reason for this increase in functional group−electrode interactions is related to the chemical nature of these electrode materials. The difference in nonmetallic (graphite), semiconductor (silicon), and metallic (lithium) properties changes the interatomic bonding characteristics from covalent bonding to metallic bonding, increasing the interatomic interactions and allowing the electrode surface atoms to move more freely and approach the SPE polymer functional groups in the most convenient orientation. In conclusion, it is thus the interactions of electrode surface atoms that determine the strength of functional group−electrode interactions and the subsequent reactivity.

Investigating the Coordination Chemistry of Functional Groups to Shed Light on the Accessibility. To quantify the interactions of the electrode surface atoms, the pair correlation function $g(r) = \frac{1}{4\pi r^2}\frac{1}{N\rho}\sum_{i=1}^{n}\sum_{j\neq i}^{N}\langle\delta(r - |r_i - r_j|)\rangle$ was calculated, which in this study signifies the probability of observing electrode atoms at a certain distance from the key SPE polymer functional group atoms (Figure S13). The corresponding distances to the first coordination shell are shown in Figure 4b for all electrode materials and functional groups. The functional group−electrode distance decreases from graphite to silicon and then lithium, following the same trends as obtained through bond length variation analysis. This shows an overall repulsion caused by graphite yet an increasing affinity toward silicon and notably lithium on which the carbonyl oxygen atoms for the ester and urethane groups have the smallest functional group−electrode distances. These findings corroborate the relative position on the MinRBC/MaxRBC plots shown in Figure 3a in which, on graphite, a general trend of more bond compression was observed, which can now be attributed to a greater repulsion to the graphite electrode surface which relates to the greater functional group−electrode distance. The greater proximity on silicon and lithium can be linked to the less negative MinRBC values and shift toward greater MaxRBC values indicating a greater affinity and reactivity due to beneficial and flexible electrode surface atom interactions, which are strongest on lithium. The increase of distance for the ether groups on silicon can be explained by considering the accessible surface area as will be explained below.

Simulation snapshots are shown for all functional groups on lithium in Figure 4c with the calculated coordination numbers in ascending order. The urethane nitrogen and ethereal oxygen atoms were not in the first coordination shell and are not included. Upon calculating the average lithium-accessible surface area for all functional group atoms (Table S1), the values were found to be proportional to the coordination numbers when also taking into account the overall steric accessibility of the functional groups, confirming that the coordination is strongly dependent on steric effects of surrounding atoms as well as the overall functional group geometry. With the greatest coordination, the ester and urethane groups both have an easily accessible planar structure, followed by the alcohol in which the hydroxyl group sticks out of the molecule backbone, and finally followed by the amine and ether with the lowest coordination in which both functional groups are part of the molecule backbone and shielded sterically by surrounding alkyl groups. The high accessibility of the ester group is most likely the reason why in the short 15 ps simulation time, the decomposition reaction was observed, as shown to the right in Figure 4c. Although the urethane group also has high accessibility, no reaction was observed, which is expected to be due to the delocalization of the nitrogen atom within the group, increasing the stability. The ether group has the lowest coordination number and

https://doi.org/10.1021/acs.jpcc.2c01144
J. Phys. Chem. C 2022, 126, 8227−8237

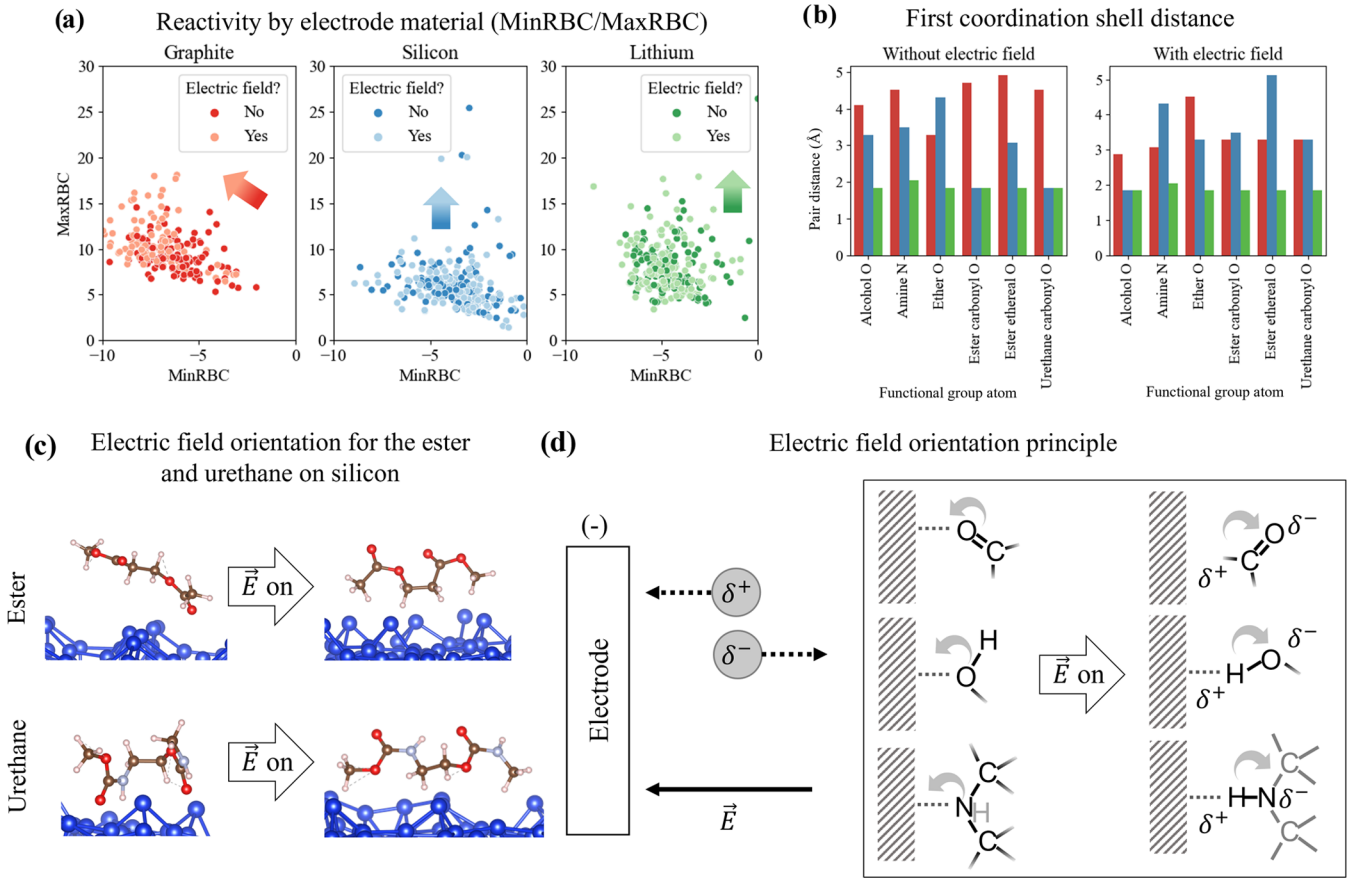

Figure 5. Influence of electric field on the reactivity and orientation of the SPE polymer molecules. (a) MinRBC/MaxRBC plots for all bond types and functional groups combined, indicating the reactivity shift in the presence of an electric field. (b) First coordination shell distance in the presence and absence of an electric field. (c) Simulation snapshots for the ester and urethane molecule on silicon illustrating the effect of electric field orientation. (d) Illustration of the electric field orientation principle.

accessibility, which causes the coordination distance to increase on silicon as shown in Figure 4b due to the inaccessibility to the surface and the low degree of interactions. On lithium, there is however a decrease, due to the surface atoms being more mobile than on silicon, and therefore more beneficially shaping the surface morphology for good interaction. In conclusion, the interactions of electrode surface atoms, combined with the accessibility of the functional groups are critical in determining the affinity and reactivity. However, environmental parameters such as the electric field and temperature are also known to influence the reactivity[42] and hence were also considered in this study.

Influence of Electric Field and Temperature on the Environmental Reactivity. Alongside the purely "chemical" reactions taking place when in rest, distinct "electrochemical" reactions occur[43] as a result of the presence of an electric field during the battery use and the subsequently induced polarization.[44] All electrode and functional group combination simulations were therefore also performed in the presence of an electric field (0.3 V/Å).

Upon visual inspection of all simulations, the functional groups were found to move closer to the electrode surface in the presence of an electric field, which resulted in a significant increase in reactivity. This decrease in the functional group−electrode distance can be explained by observing the leftward shift on graphite (Figure 5a) when exposed to an electric field, indicating a greater surface repulsion and reactivity. On the contrary, on silicon and in particular on lithium, an increase toward MaxRBC was observed, also indicating a greater reactivity, yet with no shift toward greater negative MinRBC, although these shifts are less pronounced than the one observed on graphite. This can be explained by considering the electrode surface atom interactions, which are greater for silicon and especially lithium, further increasing the number of beneficial interactions rather than causing more repulsion to the electrode surface. MinRBC/MaxRBC plots for separate bond types are shown in Figure S14 The ModeRBC also showed similar trends (Figure S15). Based on Bader net atomic charge analysis (Figure S16), the functional group O and N atoms were found to become more negative on graphite, indicating greater functional group−electrode interactions. On silicon and lithium, there were less differences due to there already being a small electrode−functional group distance due to the stronger interactions with the electrode surface even in the absence of an electric field. 3D charge density difference plots (Figures S8−S12) also confirmed an increase in the interactions, with a greater charge density difference observed in the presence of an electric field and increasing from graphite to lithium.

To investigate the influence of the electric field on the distance of the electrode surface to the key functional group atoms, the first coordination shell distance was calculated (Figure 5b). The decrease in functional group−electrode distance as observed visually in the simulation snapshots is also

https://doi.org/10.1021/acs.jpcc.2c01144
J. Phys. Chem. C 2022, 126, 8227−8237

observed through this quantitative analysis. However, very significantly, this was not the case for the amine, ester, and urethane molecules on the silicon electrode, in which upon applying an electric field, the first coordination shell distance increased. Upon visual investigation, it was found that the amine and carbonyl groups rotated to face away from the electrode surface, and not toward, which instead had been observed in the simulations without the application of an electric field. This phenomenon is shown in Figure 5c for the ester and urethane. On graphite and lithium, this behavior was not observed.

The reason for this change in orientation, and why it only occurs on silicon and not on graphite or lithium can be explained by considering two factors: (1) the partial charges of the atoms within the functional groups and their behavior toward the electric field lines and (2) the strength of the functional group−electrode interactions that influences the freedom of movement of the functional group. This concept is illustrated in Figure 5d. When considering the first factor, within the functional groups considered in this study, the O and N atoms are partially negatively charged (Figure S17). When such charges are exposed to an electric field, positive charges will undergo an acceleration following the electric field lines, which in this case point toward the electrode, which represents the charging state of a battery. Negative charges will undergo acceleration in the opposite direction. Because the atoms are connected through bonds, this will result in a change in the orientation of the bonds. The effect was found to be visually most pronounced for carbonyl groups, which can orient more freely due to the presence of more polarizable π-electrons, which could result in a dipole prone to orienting to the electric field.[43] Considering the second factor, the strength of functional group−electrode interactions influences the freedom of movement of the functional group on the surface. On graphite, due to its planar structure, molecules rotate and move freely over the electrode surface. In this case, the kinetic energy is very high and stronger than the force orienting it to the electric field, resulting in no selective orientation of the functional groups. On lithium, the interactions are very strong and lithium atoms are able to move outward, anchoring the functional groups in place, preventing any freedom of movement, and thus here also making it impossible for the functional groups to selectively orient to the electric field lines. However, on silicon, there is neither a planar structure nor the functional group−electrode interactions are very strong, and it is this balance that allows for the functional groups to orient toward the electric field lines.

Because of this balance in the kinetic (freedom of movement depending on both the electrode properties and the temperature) and thermodynamic (strength of the electric field) effects, the effect of electric field orientation is expected to be stronger for low-temperature and high-electric field environments. With a reported lack of studies on the effects of low temperatures and high electric fields (high current density-induced, such as in fast-charging applications),[23] this merits a further investigation in future studies and this phenomenon could potentially be used to devise new approaches to improve the electrode−electrolyte stability.

Because the kinetic and thermodynamic parameters are strongly influenced by the temperature and electric field strength, respectively, it is worth considering the influence of such elevated conditions. The application of lithium batteries in more energy-intensive applications such as electric vehicles and fast-charging technologies means that greater current densities will lead to stronger electric fields at the electrode surface. To verify the influence of this, additional simulations for the ester molecule given its high reactivity were performed at 0.6 V/Å, twice the strength of the previously used electric field. The RBC analysis results (Figure S18) show an even greater shift toward more negative MinRBC and positive MaxRBC values for 0.6 V/Å, especially for graphite. On lithium, the shift is less apparent, which can be explained by the already stronger SPE polymer-electrode affinity in the absence of an electric field. On silicon, due to the electric field orientation effect, the reactivity decreased slightly. As observed in this study, stronger electric fields are expected to decrease the functional group−electrode distance, which increases the number of interactions and is expected to lead to increased long-term reactivity. The functional group−electrode distance was calculated (Figure S19) through the pair correlation function, which confirmed the same observations as for the 0.3 V/Å simulations in that there was a decrease in graphite and no significant change in lithium, with a significant increase in silicon, further confirming the electric field orientation effect.

Finally, the influence of the temperature was investigated. Previously analyzed simulations were conducted at 400 K (127 °C) to reduce simulation time. For a more realistic temperature, additional simulations were performed at 300 K for the ester molecule, given its higher reactivity, on all electrode types and both in the presence and absence of an electric field (0.3 V/Å). A shift toward less negative MinRBC and less positive MaxRBC was observed (Figure S20) on all electrode materials at a lower temperature in the absence and presence of an electric field, confirming that at a higher temperature, the reactivity increases. The increase was also observed in ModeRBC (Figure S21).

In summary, in the presence of an electric field, the functional group−electrode distance decreases, increasing the number of interactions and therefore also the reactivity. Furthermore, the kinetic−thermodynamic trade-off causes functional groups to selectively orient along the electric field lines. This balance was found to be present for silicon yet not for graphite and lithium. Experimental confirmation and a thorough review of the factors influencing this trade-off may lead to new electrode materials which allow for an even greater control of the interfacial stability. Increases in the reactivity at an elevated electric field strength and temperature were confirmed. Whether these increases have an influence on the selectivity of the altered reactivity merits a further investigation in future studies and could potentially lead to new approaches to design compatible, high-performance, and durable electrode−electrolyte interfaces.

CONCLUSIONS

As part of one of the key development points toward obtaining high-performance and long-lifetime rechargeable batteries and with the latest advances in fast-charging and high current density applications, as well as with the use of lithium metal electrodes, electrolyte−electrode interfaces are facing even greater challenges in which controlling the reactivity, limiting where possible, and promoting controlled solid−electrolyte interphase layers are key to obtaining stable and long-lifespan batteries. Given the complexity of these interface systems, having more accessible, accurate, and less costly simulation-interpretation methods such as the bond length analysis

https://doi.org/10.1021/acs.jpcc.2c01144
J. Phys. Chem. C 2022, 126, 8227−8237

method explained in this study will allow us to further the progress on battery development with greater efficiency.

This study has both introduced a new approach to assess the long-term reactivity and applied this to a practical application of the electrolyte−electrode interface. A thorough analysis of the bond length variation distributions has been proven to be able to provide a long-term reactivity forecast based on short-timespan AIMD simulations. By applying this technique to different electrode material combinations and environments, key factors in determining the reactivity have been discovered. The surface morphology, strength of interactions of electrode surface atoms, and the accessibility of the functional groups were found to be critical factors in determining the strength of electrode−functional group interactions and the subsequent affinity and reactivity. The presence of an electric field was found to decrease the functional group−electrode distance, increasing the number of interactions and therefore also the reactivity. Increases in the reactivity at an elevated electric field strength and temperature were also confirmed. The newly elucidated kinetic−thermodynamic trade-off was found to cause functional groups to selectively orient along the electric field lines in particular on silicon, where this balance was achieved at the given temperature.

In future studies, it will be worth investigating whether changes in the temperature and electric field strength alter not only the reactivity but also their selectivity. Additionally, alongside the SPE polymer, the electrolyte salt is known to significantly influence the electrochemical stability of the SPE,[45] which merits a further investigation into changes in the interfacial stability of the SPE polymer and electrolyte salt in combined systems using the RBC approach. With the electric field orientation principle, experimental confirmation and a thorough review of the factors influencing this trade-off will lead to new insights and electrode materials, which will allow for an even greater control of the interfacial stability and leading to new insights, which could contribute to the design of compatible, high-performance, and durable electrode−electrolyte interfaces. Furthermore, the obtained knowledge on how reactive key SPE polymer functional groups are and also how their reactivity changes in terms of the electric field orientation effect could be used to design new stable SPE polymers in which the choice of functional groups results in both an optimized high ionic conductivity and interfacial stability. Finally, this technique could also be applied to other domains, both in solid-state and liquid-state batteries, and beyond in chemical and biochemical areas in which the influence of different chemical environments on the reactivity of molecules is of interest, such as the influence of interfaces, solvation, and environmental parameters such as temperature, pressure, electric field strength, etc.

■ ASSOCIATED CONTENT

Supporting Information

The Supporting Information is available free of charge at https://pubs.acs.org/doi/10.1021/acs.jpcc.2c01144.

Additional information concerning all simulations and analyses (PDF)

■ AUTHOR INFORMATION

Corresponding Author

Frank De Proft − *Eenheid Algemene Chemie (ALGC), Vrije Universiteit Brussel (VUB), 1050 Brussels, Belgium;* orcid.org/0000-0003-4900-7513; Email: fdeprof@vub.be

Authors

Lieven Bekaert − *Research Group Electrochemical and Surface Engineering (SURF), Department of Materials and Chemistry, Vrije Universiteit Brussel, 1050 Brussels, Belgium; Eenheid Algemene Chemie (ALGC), Vrije Universiteit Brussel (VUB), 1050 Brussels, Belgium;* orcid.org/0000-0003-1776-1888

Ashish Raj − *Institute of Condensed Matter and Nanosciences, Université Catholique de Louvain, 1348 Louvain-la-Neuve, Belgium*

Jean-François Gohy − *Institute of Condensed Matter and Nanosciences, Université Catholique de Louvain, 1348 Louvain-la-Neuve, Belgium;* orcid.org/0000-0003-4169-1883

Annick Hubin − *Research Group Electrochemical and Surface Engineering (SURF), Department of Materials and Chemistry, Vrije Universiteit Brussel, 1050 Brussels, Belgium*

Mesfin H. Mamme − *Research Group Electrochemical and Surface Engineering (SURF), Department of Materials and Chemistry, Vrije Universiteit Brussel, 1050 Brussels, Belgium; Eenheid Algemene Chemie (ALGC), Vrije Universiteit Brussel (VUB), 1050 Brussels, Belgium*

Complete contact information is available at: https://pubs.acs.org/10.1021/acs.jpcc.2c01144

Author Contributions

The manuscript was written through contributions of all authors. All authors have given approval to the final version of the manuscript.

Notes

The authors declare no competing financial interest.

■ ACKNOWLEDGMENTS

L.B. acknowledges funding from the Research Foundation—Flanders (FWO, Project 1151522N). L.B. and A.R. acknowledge funding from Innoviris (Project 2019-RPF-8). M.H.M. acknowledges funding from the Research Foundation—Flanders (FWO, Project 1264221N). The computational resources and services used in this work were provided by the VSC (Flemish Supercomputer Center), funded by the Research Foundation—Flanders (FWO) and the Flemish Government.

■ ABBREVIATIONS

RBC, relative bond length change; SSE, solid-state electrolyte; SPE, solid polymer electrolyte; AIMD, ab initio molecular dynamics; DFT, density functional theory; ARXPS, angle-resolved X-ray photoelectron spectroscopy

■ REFERENCES

(1) Goodenough, J. B.; Park, K.-S. The Li-Ion Rechargeable Battery: A Perspective. *J. Am. Chem. Soc.* **2013**, *135*, 1167−1176.

(2) Goodenough, J. B.; Kim, Y. Challenges for Rechargeable Li Batteries. *Chem. Mater.* **2010**, *22*, 587−603.

(3) Albertus, P.; Babinec, S.; Litzelman, S.; Newman, A. Status and Challenges in Enabling the Lithium Metal Electrode for High-Energy and Low-Cost Rechargeable Batteries. *Nat. Energy* **2018**, *3*, 16−21.

(4) Lin, D.; Liu, Y.; Cui, Y. Reviving the Lithium Metal Anode for High-Energy Batteries. *Nat. Nanotechnol.* **2017**, *12*, 194−206.

(5) Sun, C.; Liu, J.; Gong, Y.; Wilkinson, D. P.; Zhang, J. Recent Advances in All-Solid-State Rechargeable Lithium Batteries. *Nano Energy* **2017**, *33*, 363−386.
(6) Roy, P.; Srivastava, S. K. Nanostructured Anode Materials for Lithium Ion Batteries. *J. Mater. Chem. A* **2015**, *3*, 2454−2484.
(7) Liu, B.; Zhang, J.-G.; Xu, W. Advancing Lithium Metal Batteries. *Joule* **2018**, *2*, 833−845.
(8) Scrosati, B. History of Lithium Batteries. *J. Solid State Electrochem.* **2011**, *15*, 1623−1630.
(9) Goriparti, S.; Miele, E.; De Angelis, F.; Di Fabrizio, E.; Zaccaria, R. P.; Capiglia, C. Review on Recent Progress of Nanostructured Anode Materials for Li-Ion Batteries. *J. Power Sources* **2014**, *257*, 421−443.
(10) Zhu, C.; Han, K.; Geng, D.; Ye, H.; Meng, X. Achieving High-Performance Silicon Anodes of Lithium-Ion Batteries via Atomic and Molecular Layer Deposited Surface Coatings: An Overview. *Electrochim. Acta* **2017**, *251*, 710−728.
(11) Dou, F.; Shi, L.; Chen, G.; Zhang, D. Silicon/Carbon Composite Anode Materials for Lithium-Ion Batteries. *Electrochem. Energy Rev.* **2019**, *2*, 149−198.
(12) Bachman, J. C.; Muy, S.; Grimaud, A.; Chang, H.-H.; Pour, N.; Lux, S. F.; Paschos, O.; Maglia, F.; Lupart, S.; et al. Inorganic Solid-State Electrolytes for Lithium Batteries: Mechanisms and Properties Governing Ion Conduction. *Chem. Rev.* **2016**, *116*, 140−162.
(13) Famprikis, T.; Canepa, P.; Dawson, J. A.; Islam, M. S.; Masquelier, C. Fundamentals of Inorganic Solid-State Electrolytes for Batteries. *Nat. Mater.* **2019**, *18*, 1278−1291.
(14) Kato, Y.; Hori, S.; Saito, T.; Suzuki, K.; Hirayama, M.; Mitsui, A.; Yonemura, M.; Iba, H.; Kanno, R. High-Power All-Solid-State Batteries Using Sulfide Superionic Conductors. *Nat. Energy* **2016**, *1*, No. 16030.
(15) Kim, K.; Siegel, D. J. Predicting Wettability and the Electrochemical Window of Lithium-Metal/Solid Electrolyte Interfaces. *ACS Appl. Mater. Interfaces* **2019**, *11*, 39940−39950.
(16) Koshikawa, H.; Matsuda, S.; Kamiya, K.; Miyayama, M.; Kubo, Y.; Uosaki, K.; Hashimoto, K.; Nakanishi, S. Dynamic Changes in Charge-Transfer Resistance at Li Metal/Li7La3Zr2O12 Interfaces during Electrochemical Li Dissolution/Deposition Cycles. *J. Power Sources* **2018**, *376*, 147−151.
(17) Jung, S.-K.; Gwon, H.; Lee, S.-S.; Kim, H.; Lee, J. C.; Chung, J. G.; Park, S. Y.; Aihara, Y.; Im, D. Understanding the Effects of Chemical Reactions at the Cathode−Electrolyte Interface in Sulfide Based All-Solid-State Batteries. *J. Mater. Chem. A* **2019**, *7*, 22967−22976.
(18) Xu, K. Nonaqueous Liquid Electrolytes for Lithium-Based Rechargeable Batteries. *Chem. Rev.* **2004**, *104*, 4303−4418.
(19) Yue, L.; Ma, J.; Zhang, J.; Zhao, J.; Dong, S.; Liu, Z.; Cui, G.; Chen, L. All Solid-State Polymer Electrolytes for High-Performance Lithium Ion Batteries. *Energy Storage Mater.* **2016**, *5*, 139−164.
(20) Keller, M.; Varzi, A.; Passerini, S. Hybrid Electrolytes for Lithium Metal Batteries. *J. Power Sources* **2018**, *392*, 206−225.
(21) Yu, X.; Manthiram, A. A Review of Composite Polymer-Ceramic Electrolytes for Lithium Batteries. *Energy Storage Mater.* **2021**, *34*, 282−300.
(22) Yu, C.; Ganapathy, S.; van Eck, E. R. H.; Wang, H.; Basak, S.; Li, Z.; Wagemaker, M. Accessing the Bottleneck in All-Solid State Batteries, Lithium-Ion Transport over the Solid-Electrolyte-Electrode Interface. *Nat. Commun.* **2017**, *8*, No. 1086.
(23) Pang, M.; Yang, K.; Brugge, R.; Zhang, T.; Liu, X.; Pan, F.; Yang, S.; Aguadero, A.; Wu, B.; Marinescu, M.; et al. Interactions Are Important: Linking Multi-Physics Mechanisms to the Performance and Degradation of Solid-State Batteries. *Mater. Today* **2021**, *49*, 145−183.
(24) Car, R.; Parrinello, M. Unified Approach for Molecular Dynamics and Density-Functional Theory. *Phys. Rev. Lett.* **1985**, *55*, 2471−2474.
(25) Ebadi, M.; Marchiori, C.; Mindemark, J.; Brandell, D.; Araujo, C. M. Assessing Structure and Stability of Polymer/Lithium-Metal Interfaces from First-Principles Calculations. *J. Mater. Chem. A* **2019**, *7*, 8394−8404.
(26) Tuckerman, M. E.; Martyna, G. J. Understanding Modern Molecular Dynamics: Techniques and Applications. *J. Phys. Chem. B* **2000**, *104*, 159−178.
(27) Kresse, G.; Furthmüller, J. Efficient Iterative Schemes for Ab Initio Total-Energy Calculations Using a Plane-Wave Basis Set. *Phys. Rev. B* **1996**, *54*, No. 11169.
(28) Blöchl, P. E. Projector Augmented-Wave Method. *Phys. Rev. B* **1994**, *50*, No. 17953.
(29) Perdew, J.; Burke, K.; Enzerhof, M. Generalized Gradient Approximation Made Simple. *Phys. Rev. Lett.* **1997**, *78*, No. 1396.
(30) Grimme, S.; Ehrlich, S.; Goerigk, L. Effect of the Damping Function in Dispersion Corrected Density Functional Theory. *J. Comput. Chem.* **2011**, *32*, 1456−1465.
(31) Momma, K.; Izumi, F. VESTA 3 for Three-Dimensional Visualization of Crystal, Volumetric and Morphology Data. *J. Appl. Crystallogr.* **2011**, *44*, 1272−1276.
(32) Tang, W.; Sanville, E.; Henkelman, G. A Grid-Based Bader Analysis Algorithm without Lattice Bias. *J. Phys.: Condens. Matter* **2009**, *21*, No. 084204.
(33) Frisch, M. J.; Trucks, G. W.; Schlegel, H. B.; Scuseria, G. E.; Robb, M. A.; Cheeseman, J. R.; Scalmani, G.; Fukuda, R.; Fox, D. J. et al. *Gaussian 16*, revision A.03, 2016.
(34) Parr, R. G. Density Functional Theory of Atoms and Molecules. In *Horizons of Quantum Chemistry*; Springer, 1980; Vol. *136*, pp 5−15.
(35) Zhao, Y.; Truhlar, D. G. The M06 Suite of Density Functionals for Main Group Thermochemistry, Thermochemical Kinetics, Noncovalent Interactions, Excited States, and Transition Elements: Two New Functionals and Systematic Testing of Four M06-Class Functionals and 12 Other Functionals. *Theor. Chem. Acc.* **2008**, *120*, 215−241.
(36) Kumar, N.; Seminario, J. M. Lithium-Ion Model Behavior in an Ethylene Carbonate Electrolyte Using Molecular Dynamics. *J. Phys. Chem. C* **2016**, *120*, 16322−16332.
(37) Amanchukwu, C. V.; Kong, X.; Qin, J.; Cui, Y.; Bao, Z. Nonpolar Alkanes Modify Lithium-Ion Solvation for Improved Lithium Deposition and Stripping. *Adv. Energy Mater.* **2019**, *9*, No. 1902116.
(38) Livingston, E. H. The Mean and Standard Deviation: What Does It All Mean? *J. Surg. Res.* **2004**, *119*, 117−123.
(39) Niu, C.; Pan, H.; Xu, W.; Xiao, J.; Zhang, J.-G.; Luo, L.; Wang, C.; Mei, D.; Meng, J.; Wang, X.; et al. Self-Smoothing Anode for Achieving High-Energy Lithium Metal Batteries under Realistic Conditions. *Nat. Nanotechnol.* **2019**, *14*, 594−601.
(40) Aurbach, D.; Daroux, M. L.; Faguy, P. W.; Yeager, E. Identification of Surface Films Formed on Lithium in Propylene Carbonate Solutions. *J. Electrochem. Soc.* **1987**, *134*, 1611.
(41) Xu, C.; Sun, B.; Gustafsson, T.; Edström, K.; Brandell, D.; Hahlin, M. Interface Layer Formation in Solid Polymer Electrolyte Lithium Batteries: An XPS Study. *J. Mater. Chem. A* **2014**, *2*, 7256−7264.
(42) Wang, A.; Kadam, S.; Li, H.; Shi, S.; Qi, Y. Review on Modeling of the Anode Solid Electrolyte Interphase (SEI) for Lithium-Ion Batteries. *Npj Comput. Mater.* **2018**, *4*, No. 15.
(43) Vatamanu, J.; Borodin, O.; Smith, G. D. Molecular Dynamics Simulation Studies of the Structure of a Mixed Carbonate/LiPF6 Electrolyte near Graphite Surface as a Function of Electrode Potential. *J. Phys. Chem. C* **2012**, *116*, 1114−1121.
(44) Borodin, O. Polarizable Force Field Development and Molecular Dynamics Simulations of Ionic Liquids. *J. Phys. Chem. B* **2009**, *113*, 11463−11478.
(45) Marchiori, C. F. N.; Carvalho, R. P.; Ebadi, M.; Brandell, D.; Araujo, C. M. Understanding the Electrochemical Stability Window of Polymer Electrolytes in Solid-State Batteries from Atomic-Scale Modeling: The Role of Li-Ion Salts. *Chem. Mater.* **2020**, *32*, 7237−7246.

https://doi.org/10.1021/acs.jpcc.2c01144
J. Phys. Chem. C 2022, 126, 8227−8237